ChemPhysChem

Research Article
doi.org/10.1002/cphc.202100755

Chemistry Europe
European Chemical
Societies Publishing

www.chemphyschem.org

Temperature and Composition Dependent Optical Properties of CdSe/CdS Dot/Rod-Based Aerogel Networks

Pascal Rusch,[a, b] Denis Pluta,[a, b, c] Franziska Lübkemann,[a, b] Dirk Dorfs,[a, b, d] Dániel Zámbó,[a, b] and Nadja C. Bigall*[a, b, d]

Employing nanocrystals (NCs) as building blocks of porous aerogel network structures allows the conversion of NC materials into macroscopic solid structures while conserving their unique nanoscopic properties. Understanding the interplay of the network formation and its influence on these properties like size-dependent emission is a key to apply techniques for the fabrication of novel nanocrystal aerogels. In this work, CdSe/CdS dot/rod NCs possessing two different CdSe core sizes were synthesized and converted into porous aerogel network structures. Temperature-dependent steady-state and time-resolved photoluminescence measurements were performed to expand the understanding of the optical and electronic properties of these network structures generated from these two different building blocks and correlate their optical with the structural properties. These investigations reveal the influence of network formation and aerogel production on the network-forming nanocrystals. Based on the two investigated NC building blocks and their aerogel networks, mixed network structures with various ratios of the two building blocks were produced and likewise optically characterized. Since the different building blocks show diverse optical response, this technique presents a straightforward way to color-tune the resulting networks simply by choosing the building block ratio in connection with their quantum yield.

Introduction

With the introduction of network structures based on colloidal CdS dispersions[1,2] and the conversion of these nanocrystal-(NC) based gels to aerogels[3,4] – porous network structures – an exciting new class of materials emerged. In analogy to the well-established sol-gel method, this allows for the transformation of nanoscopic materials into macroscopic, self-supported solids.[5,6] A number of methods[3,7–12] to produce aerogel networks based on most of the available NCs[13–18] has been developed and first demonstrations of applications have been published. These were focused on the sensing[19,20] or catalytic[21–25] properties of the NC building blocks but much less attempts have been made to utilize the inherent photoluminescence (PL) of the semiconducting NC building blocks. Compared to the more classical sol-gel approach to produce aerogel networks, a key advantage of NC-based aerogels is that it allows for the synthesis of the individual NC building blocks in a separate step prior to the network formation. In turn, enabling the use of the vast library of NC synthesis and modification procedures to be used to fine-tune the building blocks and in consequence the later network itself. As these NC-based structures bridge from the nanoscopic scale of each building block up to the macroscopic shape of the resulting monolith, the tuning of their properties can similarly be performed on the level of the individual building block (e.g. shape-selective synthesis[10,26] or bandgap engineering[26,27]), and the macroscopic ensemble (e.g. patterning[28]). In addition to these nano- and macrostructuring possibilities, a level of control can also be exerted at the intermediate scale to tune the microstructure and the building block connection.[29] Multicomponent networks, formed of more than one building block material, are often used to connect semiconducting materials with metallic ones for the generation of catalytically active networks. This can be done by the isolated synthesis of two different NC building blocks,[30–34] assembling hybrid nanoparticles[35–37] or even via the direct deposition of the metal to the forming network.[38,39] The idea of connecting two different semiconducting NC building blocks into one network has been explored much less frequently. The nature of the interparticle connection,[8] the ligands[40,41] and the composition[42] play a governing role in the control over the assembled gel structures in terms of the structural as well as optical properties. When combining two differently-sized CdTe NC building blocks or CdTe and ZnSe NC building blocks which

[a] P. Rusch, D. Pluta, Dr. F. Lübkemann, Dr. D. Dorfs, Dr. D. Zámbó,
     Prof. N. C. Bigall
     Institute of Physical Chemistry and Electrochemistry,
     Leibniz Universität Hannover
     Callinstraße 3A, 30167 Hannover, Germany
     E-mail: nadja.bigall@pci.uni-hannover.de
[b] P. Rusch, D. Pluta, Dr. F. Lübkemann, Dr. D. Dorfs, Dr. D. Zámbó,
     Prof. N. C. Bigall
     Laboratory of Nano and Quantum Engineering,
     Leibniz Universität Hannover
     Schneiderberg 39, 30167 Hannover, Germany
[c] D. Pluta
     Hannover School for Nanotechnology,
     Leibniz Universität Hannover
     Schneiderberg 39, 30167 Hannover, Germany
[d] Dr. D. Dorfs, Prof. N. C. Bigall
     Cluster of Excellence, PhoenixD
     (Photonics, Optics and Engineering – Innovation Across Disciplines),
     Leibniz Universität Hannover
     30167 Hannover, Germany

ChemPhysChem

Research Article
doi.org/10.1002/cphc.202100755

Chemistry
Europe
European Chemical
Societies Publishing

differ in their band positions into one network, energy and charge transfer within these semiconductor multicomponent networks could be confirmed by the change in the emission spectra between the building block solution and the connected networks. In turn, this could then be used to tune the ratios of the different components to generate white emitting aerogels.[42]

In the present work, we aim to increase our understanding of the optical properties of these multicomponent semiconductor NC-based networks namely within the system of CdSe/CdS dot/rod NC building blocks by analyzing their temperature-dependent optical properties. The measurements are performed by steady-state as well as time-resolved photoluminescence (PL) spectroscopy. Additionally, expanding this established system of CdSe/CdS dot/rod NC-based aerogels via the use of building blocks with differently sized CdSe cores and therefore varying emission colors is also targeted, as schematically drawn out in Figure 1A. These systems of connected CdSe/CdS dot/rod NCs are remarkable due to their optical properties, i.e. the difference in PL lifetimes at the level of the individual building blocks and a connected network.[8] The measured PL decay of the connected network is considerably longer than the decay of the isolated particles which could be attributed to the interparticle connection and a resulting delocalization of the excited electron over several connected building blocks.[8,43]

Results and Discussion

Optical Properties of CdSe/CdS Dot/Rod Building Blocks and Their Aerogel Networks

The nanocrystal building blocks were synthesized along well-known literature routes by hot injection method (see Experimental Section for details). To this end, CdSe QDs in two sizes were produced. For the sake of simplicity, these will be called small core for 2.0 nm CdSe QDs and large core for 3.9 nm CdSe QDs in the following. These CdSe QDs were then used as seeds

Figure 1. Schematic depiction of (A) the synthesis route of the investigated CdSe/CdS NC-based aerogel networks and (B) the band structure of the two NCs based on differently sized CdSe cores.

for the growth of an elongated CdS shell, which resulted in the production of CdSe/CdS dot/rods with dimensions of ca. 4× 50 nm independent of the CdSe core size (see Figure 2A,B and S1) The ensemble optical properties (see Figure 2E,F) were tuned via the size of the CdSe core embedded into a CdS shell showing a size-dependent CdSe absorption maxima at 537 nm (small core) and 605 nm (large core) and the emission at 555 nm and 608 nm for CdSe/CdS dot/rods, respectively. For both heteroparticle systems, a strong absorption can be observed below 500 nm due to the band edge of the CdS shell material accounting for the majority of the dot/rods.

These well-defined dot/rod building blocks were then assembled into interconnected porous network structures (i.e. gels) by controlled oxidative removal of their protective ligands (3-mercaptopropionic acid) via the addition of low concentrations of hydrogen peroxide (see Figure 2C,D). This process favorably attacks the ligands on the NC tips (due to steric considerations) and also facilitates the generation of sulfur-sulfur bonds resulting in the NCs forming a mostly tip-to-tip connected crystal-crystal bound network.[8] As has been shown in earlier works, these networks show considerably longer PL lifetimes compared to their individual NC building blocks. This effect was previously attributed to the delocalization of excited electrons within several connected building blocks, thereby decreasing electron-hole overlap.[8] As can be seen in Figure 2F, this effect is also clearly visible in the large core sample for this study with the PL lifetimes increasing from 15 ns for individual building blocks to 28 ns in the network structure. In the small core sample, the increase in PL lifetime between individual NCs and an interconnected network is likewise observed with an increase of the PL lifetime from 22 ns to 29 ns. This confirms the influence of the interconnection of the CdSe/CdS dot/rod building blocks as well as the conduction band-offset between the combined semiconductors on the PL decay behavior similarly to the earlier reported red-emitting CdSe/CdS dot/rod based aerogel networks.[8] Networks build-up from building blocks based on much smaller CdSe cores not investigated yet. This is interesting as these smaller CdSe core-based structures have been reported to behave differently to larger CdSe core-based ones in certain aspects. With smaller CdSe cores and as consequence a larger bandgap of the core material, the conduction band offset between the CdSe core and the CdS shell is expected to decrease (see scheme in Figure 1B), leading to an increased leaking of the electron wavefunction into the CdS shell in the excited dot/rod.[44–47] This leads to longer PL lifetimes in CdSe/CdS dot/rods with smaller cores due to the increased delocalization of the excited electron. Meanwhile, the steady-state optical properties (see Figure 2E) of these CdSe/CdS dot/rod-based aerogel networks are similar to their building blocks. The CdSe absorption is clearly visible at 525 nm (small core) and 590 nm (large core) with the CdS absorption edge around 480 nm in both instances. As can be seen in the spectra, the absorption of the network structures reaches a saturation around this CdS band edge whereby higher energy of the incident light does not lead to a higher measured absorption – as would be the case for diluted dispersions of the building blocks. This is due to the optically dense sample being
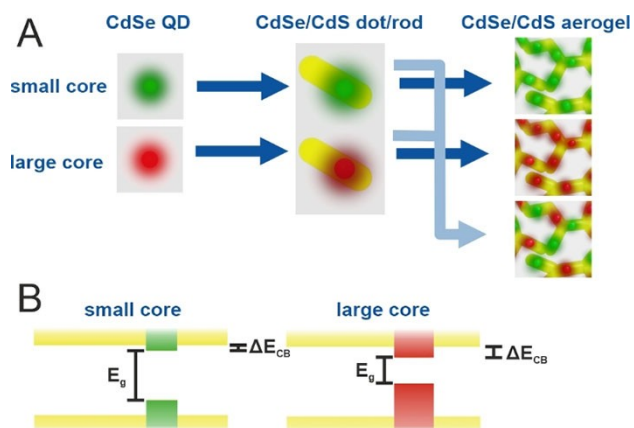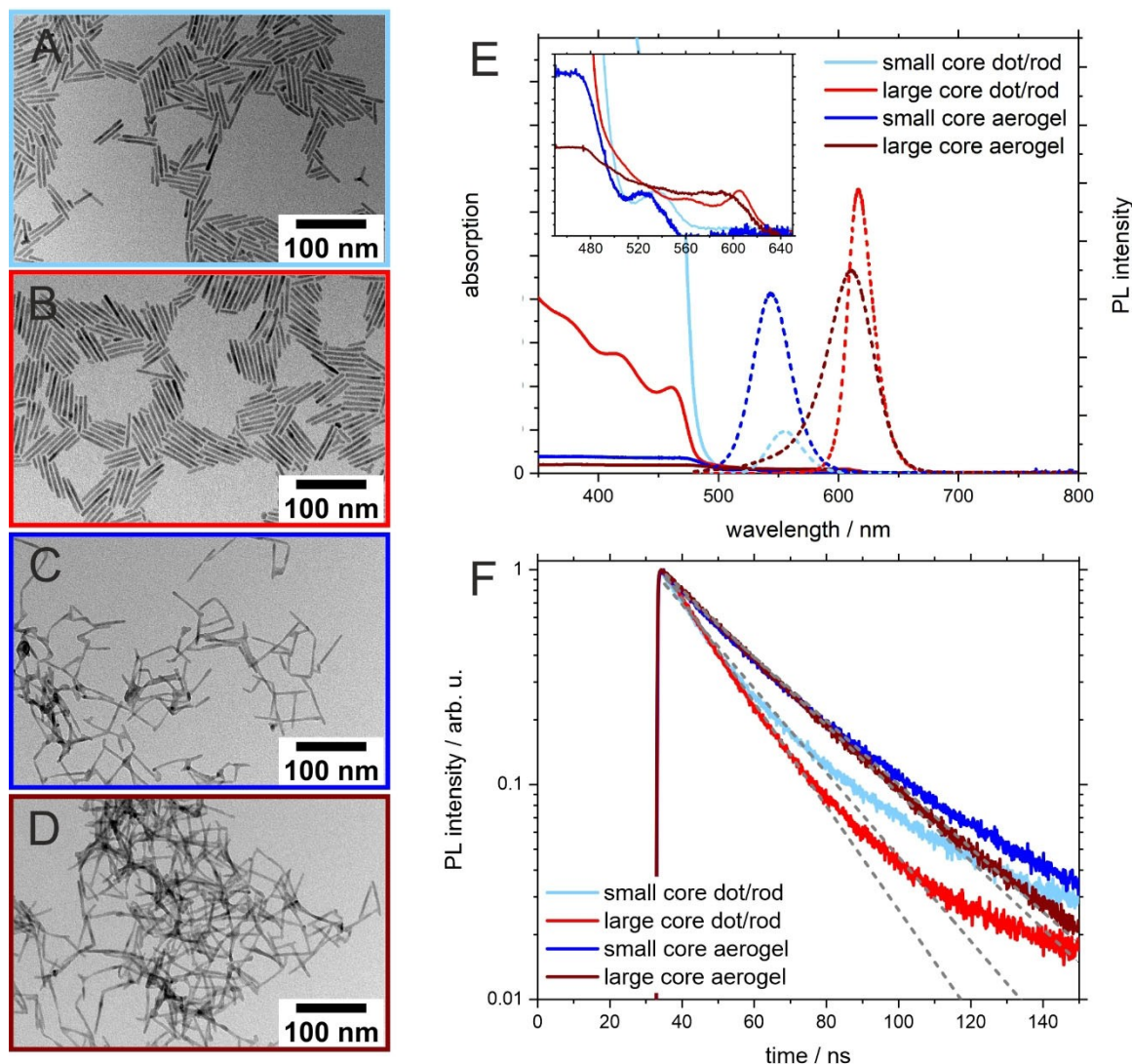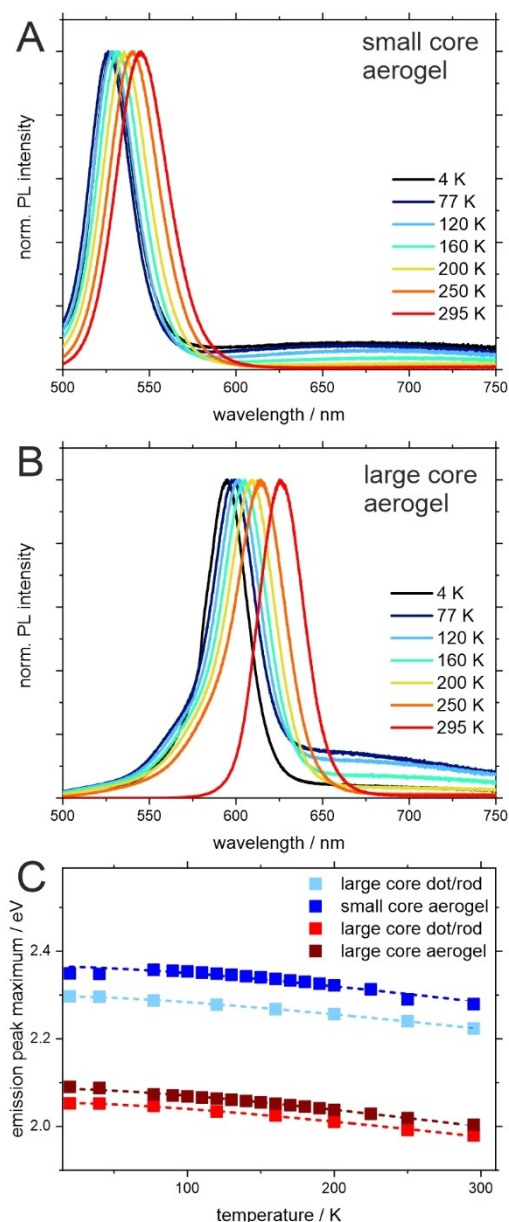
Figure 2. CdSe/CdS dot/rod NC-based aerogel network structures and the individual building block NCs. TEM micrographs of CdSe/CdS dot/rod NCs synthesized from (A) 2.0 nm CdSe cores and (B) 3.9 nm CdSe cores and the respective (C, D) network structures. (E) Absorption (solid lines) and emission (dashed lines) spectra with inset showing the magnified area of CdSe absorption and (F) PL decays of these CdSe/CdS dot/rod NC-based aerogel networks and the individual building blocks (2.0 nm CdSe core-based structures in blue colors, 3.9 nm CdSe core-based structures in red colors).

a macroscopic monolith comparable to a very highly concentrated dispersion. Like their building blocks, the assembled network structures show emission from the CdSe core at 544 nm and 608 nm respectively. The PL quantum yield (PLQY) increases from 6% (small core) and 23% (large core) in the respective aqueous dispersions to 26% (small core) and 38% (large core) in the aerogels (see Figure S6). This increase in PLQY is most likely caused by the removal of solvent and therefore a removal of certain non-radiative recombination pathways.[48,49] Additionally, by the crystal-to-crystal connection of the inorganic building blocks *via* the tips, surface traps on the tips are likely to be eliminated.

Temperature Dependent Optical Properties of CdSe/CdS Dot/Rod Aerogel Networks

The aerogel networks, as well as their building blocks as a reference, were then systematically investigated with regards to their optical properties at lower temperatures. The steady-state emission spectra change consistently with the changing temperature for the network structures and their building blocks (see Figure 3 and S3). The emission maxima shift to higher energy at lower temperatures accompanied by a decreasing full width at half maximum (FWHM). These parameters can be extracted from the experimental spectra by fitting with a single Gaussian. This temperature-dependent emission behavior is well-known and documented for semiconducting NCs[50–52] and can be attributed to exciton-phonon coupling as well as lattice deformation both being temperature-dependent

ChemPhysChem

Research Article
doi.org/10.1002/cphc.202100755

Chemistry Europe
European Chemical
Societies Publishing

Figure 3. Change of PL with temperature. Temperature dependent emission spectra of CdSe/CdS dot/rod NC-based aerogel networks with (A) CdSe core diameter of 2.0 nm and (B) CdSe core diameter of 3.9 nm. (C) Change in emission maxima depending on temperature and Varshni law fit for CdSe/CdS dot/rod NC-based network structures with different CdSe core sizes (blue colors for small cores, red colors for large cores) and the respective individual building blocks.

themselves and influencing the electronic properties of the NCs. The temperature dependent emission maxima, i.e. bandgap ($E_g(T)$), can be fitted by the empirical Varshni law[53] (Equation 1).
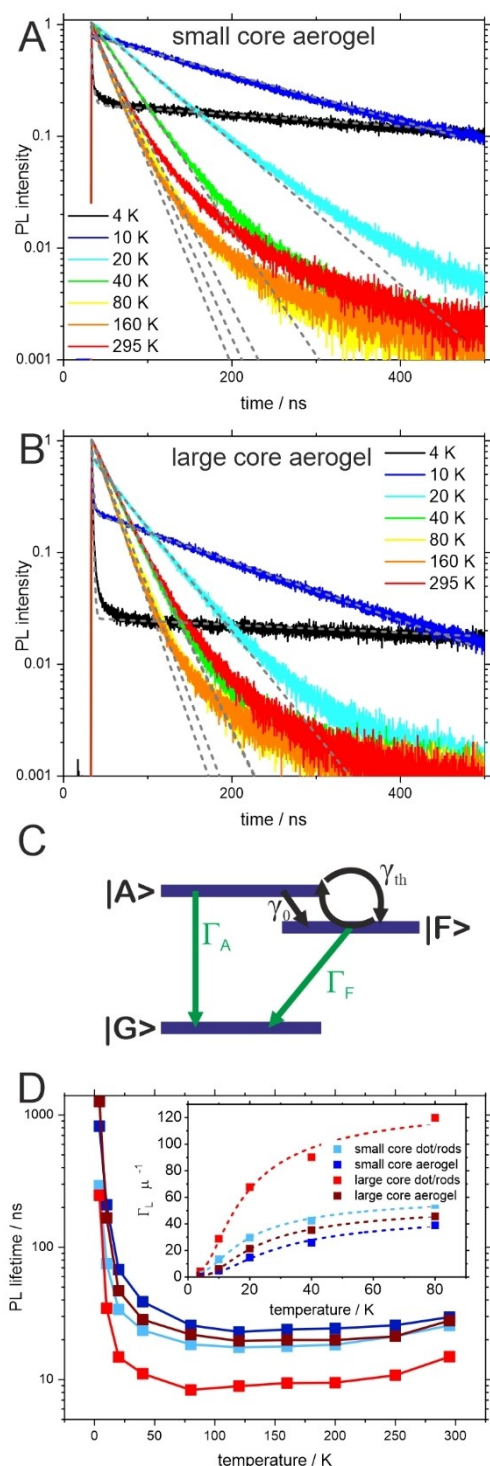
$$E_g(T) = E_g(T=0) - \frac{\alpha T^2}{(T+\beta)} \quad (1)$$

The thermal dependency of the respective emission maxima can be fitted by the Varshni law using 195 K as β (which is

roughly the Debye temperature) and ca. $4 \cdot 10^{-4}$ as α (a measure for the electron-phonon coupling) for individual NC building blocks and their networks alike (see Figure 3C), yielding values close to the ones reported for these CdSe/CdS dot/rods before.[52] The theoretical bandgap at 0 K ($E_g(T=0)$) as determined by this fit agrees well with the observed emission colors, while a slight difference between building blocks and assembled networks can be observed (see Table S1).

Looking at the time-resolved PL spectroscopy, the CdSe cores (see Figure S4) show a non-monoexponential decay behavior at higher temperatures, probably due to the lack of surface passivation. After the growth of CdS shells, the PL decay is much closer to a mono-exponential behavior, which would be expected for an ideal system. A longer decay component tail can be observed. This has been seen in the past for these types of core-shell NC systems and has been attributed to shallow electron traps causing a delayed emission.[54] For all samples, building blocks and networks alike, a similar trend can be observed with the PL lifetimes decreasing with decreasing temperature (see Figure 4 and S5). This phenomenon has been discussed in literature for the CdSe/CdS dot/rod system[51] (which are employed here as individual building blocks) but has not been investigated for the resulting network structures, yet. For the building blocks, several different factors have been argued to cause this behavior of decreasing PL lifetimes at lower temperatures, starting with (i) a shifting conduction band offset altering the extend of delocalization into the CdS shell,[51] (ii) the thermal lattice fluctuations introducing asymmetry in electron and hole wavefunction,[52] and (iii) the contribution of higher excited electron states by thermal mixing.[52] All of these proposed mechanisms would alter the electron-hole overlap which results in a change in radiative lifetimes. These effects described for the individual building blocks can be assumed to likewise take place in their interconnected network structures, and similar trends in the change of PL lifetimes with temperature can be observed for both different CdSe core sizes. Interestingly, the PL lifetimes observed for the aerogel network structures exceed the ones of the individual building blocks over the full temperature range.

The effect detailed above of decreasing PL lifetimes with decreasing temperature can be observed until roughly a temperature of 80 K. Below this and down to temperatures of 20 K a different trend can be seen with the lifetimes increasing again with decreasing temperature and easily surpassing the lifetimes measured at room temperature (see Figure 4). With continuously lower temperatures down to 4 K, the evolution of two separated processes (one with very short lifetimes and one with extremely long lifetimes) is found. As shown in Figure 4D, the measured PL lifetime decreases from initially 15 ns at room temperature to 8 ns at 77 K in case of large core dot/rods and below this temperature rises again, to then split up into two distinct processes. For clarification, it should be noted that deviation from ideal mono-exponential behavior at higher temperatures, as can be seen in some cases (see Figure 4, S4, S5) can be attributed to surface states, as has been stated earlier,[54] and should not be confused with the processes at cryogenic temperatures. Similarly, the measured PL of large

ChemPhysChem

Research Article
doi.org/10.1002/cphc.202100755

Chemistry
Europe

European Chemical
Societies Publishing

Figure 4. Temperature-dependent time-resolved PL properties. PL decay and single exponential fits at different temperatures of CdSe/CdS dot/rod NC-based network structures with (A) 2.0 nm CdSe core diameter and (B) 3.9 nm CdSe core diameter, grey lines indicate the exponential fit of the data. (C) Three-level model used to describe the PL kinetics at cryogenic temperatures. (D) Temperature-dependent PL lifetime extracted by single exponential fit (at T > 10 K) or single exponential fit of the long decay component (4–10 K), inset shows the fit of the extracted lifetimes following equation 3 (derived from a three-level model).

core aerogels decrease from 28 ns (room temperature) to 22 ns (120 K) to then increase and split into the aforementioned two processes. This behavior is also seen in the small core samples with PL lifetimes decreasing from 22 ns and 29 ns at room temperature to 18 ns and 26 ns at 77 K for small core dot/rods and SC aerogels, respectively. Again, below 77 K the increase in PL lifetime and eventual evolution of two processes can be observed for the small core samples. The transition point from PL lifetimes decreasing with decreasing temperature to then increase with decreasing temperature, i.e. the minimum measured PL lifetime, is slightly different between samples within the region of 77–120 K. The fast process of the cryogenic decays at 4 K shows lifetimes between 2.7 ns (large core dot/rods) and 1.2 ns (large core aerogels), while the slow process varies between 247 ns (in large core dot/rods) and 1262 ns (in the respective large core aerogels). Comparable results are obtained for the small core sample with a fast component, 2.4 ns (small core dot/rods) and 2.2 ns (small core aerogels), and a slow component, 292 ns (small core dot/rods) and 822 ns (small core aerogels). Similar to these observations, two processes have been shown for CdSe/ZnS NCs in the past[55] and have been attributed to the bright and dark exciton (with the first showing extremely fast recombination and the latter showing very slow recombination due to the spin forbidden transition). This behavior is very much alike in the CdSe/CdS dot/rod building blocks as has been shown in reference,[51] and in their network structures as observed in the present work. As has been demonstrated in the past,[55,56] these systems can be explained by a three-level model with the ground state ($|G>$), the bright, allowed state ($|A>$) and the dark, forbidden state ($|F>$) (see Figure 4C). The two excited states are different in energy by ΔE, the bright-dark splitting. They exhibit respective radiative recombination rates (Γ_A and Γ_F) with a spin-flip from bright to dark state denoted by γ_0 and a thermally induced spin-flip $\gamma_{th} = \gamma_0 N_B$ mixing bright and dark states with $N_B = 1/(e^{\Delta E/k_B T} - 1)$ being the Bose-Einstein phonon occupation. As has been detailed elsewhere,[56] under the assumption of the PL signal being proportional to ($\Gamma_A \rho_A + \Gamma_F \rho_F$), with the time-dependent populations of the bright (ρ_A) and dark (ρ_F) exciton states an expression for the PL signal ($S(t)$) can be derived (Equation 2).

$$S(t) = \frac{\Gamma_A N_B + \Gamma_F}{1 + 2N_B} e^{-\Gamma_L t} + \frac{\Gamma_A}{2(1 + 2N_B)} e^{-\Gamma_s t} \qquad (2)$$

In this equation, the long (Γ_L) and short (Γ_s) component of the observed PL decay can be expressed as follows:[56]

$$\Gamma_L = \frac{\Gamma_A + \Gamma_F}{2} - \frac{\Gamma_A - \Gamma_F}{2} tanh\left(\frac{\Delta E}{2k_B T}\right) \qquad (3)$$

$$\Gamma_s = \gamma_0 (1 + 2 N_B) \qquad (4)$$

This results in biexponential decays at very low temperatures with a short component caused by recombination from the bright state before relaxation and a long component caused by the recombination from the dark state. At higher temper-

atures, this transforms into a mono-exponential decay. This expression (Equation 3) can be used to fit the experimentally observed slow component of the PL decay to extract the bright-dark splitting ΔE as well as the radiative recombination rates of the bright (Γ_A) and the dark (Γ_F) state (see Figure 4D and Table S3). The CdSe/CdS building blocks show cryogenic decay curves quite similar to their respective initial CdSe cores. The domination of the PL behavior at cryogenic temperatures by the CdSe cores can be expected due to the recombination taking place solely in these cores. Minor differences might be caused by the CdS shell as this alters surface passivation and dielectric surrounding of the cores in the dot/rods. However, interestingly, as seen in the present work, the assembly of these CdSe/CdS dot/rod building blocks into aerogel networks results in increased PL lifetimes not only at room temperature but at all temperatures down to 4 K. This is unexpected so far, as the assumption for these network structures would likewise be a domination of the CdSe core in the PL decay behavior at cryogenic temperatures, if these cores are unaffected by the network assembly and drying procedure generating the aerogels. While it has been shown that the cryogenic PL decay of CdSe/CdS dot/rods depends strongly on the nanorod width, the nanorod length has shown no noticeable influence.[56] Comparing these observations to the networks in this study, the connection of the dot/rod building blocks into network structures should yield similar results as elongating the rod further. As can be seen, the width of the network structure corresponds well to the width of the individual building blocks (see Figure S1 and S2). A change in width can therefore be excluded as the reason for the difference in cryogenic decay behavior between building blocks and networks. This might in turn hint at additional processes taking place during the drying process. In the first description of CdSe/CdS dot/rod NC-based aerogel networks, the difference in decay behavior between the freshly assembled hydro- and acetogels to the dried aerogels was monitored. It was attributed to the removal of the solvent and potential sintering processes improving the connection of the building blocks to each other during the supercritical drying, which takes place at elevated pressure and slightly elevated temperature.[8] These processes, elevated pressure leading to sintering as well as the washing process during solvent exchange (which is part of the synthetic process to produce such dried aerogels), can principally all influence the surface of the NC building blocks resulting in differences in surface passivation and therefore modified PL kinetics. The cryogenic PL decay measurements presented here might also hint at these processes influencing not only the interparticle connection but likewise the internal structure of the building blocks, e.g. the CdSe to CdS interface.

Optical Properties of Aerogel Networks Assembled from Two Different CdSe/CdS Building Blocks

For further insight into the interaction between the individual building blocks inside of these CdSe/CdS network structures the two building blocks described above (small core and large core)

were then combined into one network, varying the mixing ratio of these two components. The mixing of two CdSe/CdS dot/rods possessing different emission colors in colloidal solution resulted in a colloidal mixture exhibiting both emission features (Figure 5A). The resulting spectra were fitted with a system of two Gaussians with the parameters for the peaks (peak maximum and FWHM) taken from the Gaussian fit of the emission spectrum of the individual respective dot/rods or their corresponding network structures. The area of the two peaks in the mixtures is therefore left as the only free parameter. From the ratio of the respective peak areas in combination with the PLQY of the unmixed samples, an estimation of the ratio of the two building blocks can be made (see Figure 5D and Table S4). From this ratio, a small systematic error is visible slightly shifting these ratios compared to the targeted ratios, most likely due to the error in calculating the particle concentration (using the Cd^{2+} concentration, the NC size as measured from transmission electron microscopy (TEM) and the bulk density of CdS). For the building block mixtures, as one would expect for these low concentration colloidal solutions, in which the NC building blocks can be assumed to be isolated from each other, no interaction between the two building blocks could be observed. The ratios, interestingly, could be found in the respective mixed networks with only minor deviations between mixed colloids and the mixed interconnected network (see Figure 5, for the intermediate acetogels see Figure S7). The evaluation of the emission intensity by fitting with two Gaussians worked reasonably well for all but one sample. In this instance, the fitting was not possible for the assembled networks with a high content of red-emitting (large core) building blocks (targeted ratio: 1–10). This is caused by the overlap of the more intense red emission peak and the low intensity green emission peak in conjunction with slight deviations from the ideal Gaussian peak shape. These factors did not allow for a correct fitting of the emission curve with a combination of two Gaussians. Earlier reports on other mixed semiconductor NC aerogel systems indicate a shift of emission in the case of a network consisting of two different sized CdTe QDs due to charge and energy transfer from the larger bandgap building block to the small bandgap building block which in that case needed to be taken into account upon color tuning the aerogel monolith.[42] This is very much not the case in the structures described in this work, with no strong difference between a mixture of two building blocks emitting different colors and the network assembled from them. This can be explained by the CdS shell of the building blocks. While the excited electron is delocalized over multiple connected rods as discussed earlier, the localization of the hole to the CdSe core of the building block is happening within less than 1 ps.[44,57] The recombination, therefore, happens solely in the cores after a few ps.[58] The emission color staying rather constant between the colloidal mixture of CdSe/CdS building blocks and their assembled networks does allow for a less complex approach to the color tuning of the resulting macroscopic network structures. This can be done simply by varying the ratios of the building blocks used in accordance with their quantum yields as demonstrated here with a color space from red to yellow to green (see Figure 5B).
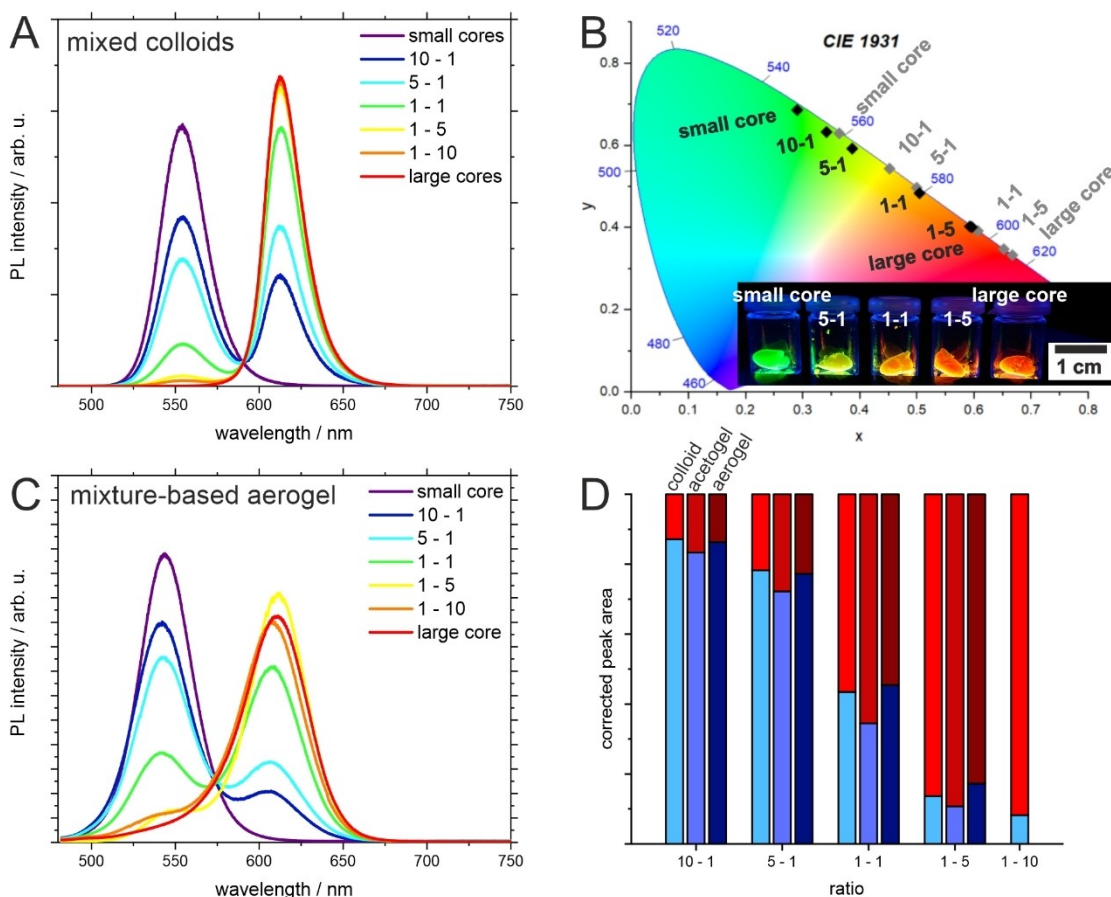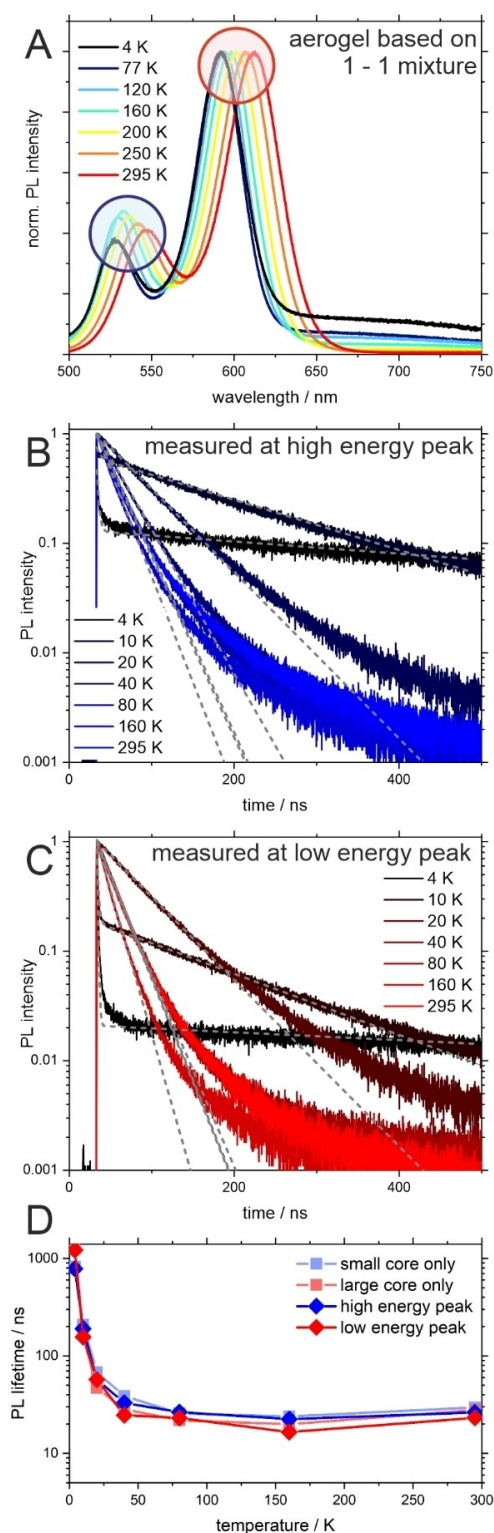
Figure 5. Emission properties of CdSe/CdS dot/rod-based network structures with two different CdSe core sizes and their mixtures (targeted molar ratios of the two mixed building block NCs are given). Emission spectra of (A) colloidal dispersions and mixtures of the building block NCs and (C) the resulting aerogel networks. (B) Chromaticity coordinates of the colloidal mixtures (grey) and the aerogels (black), inset shows a photograph of the aerogels under UV illumination. (D) Contribution to emission peak areas of the mixed colloidal NC and network structures of the small CdSe core (blue colors) and large CdSe core (red colors) NCs corrected by the quantum yield of the unmixed samples. As discussed in the main text, the evaluation of the peak areas for 1–10 ratio was only possible in colloidal mixtures.

The networks formed from different mixed building blocks also show the behavior observed for single component networks when investigating their temperature dependent optical properties (see Figure 6). The emission maxima shift and the FWHMs narrow with lower temperature. Additionally, a prominent shift in the ratio of the two emission peaks is visible. The change of emission intensity with temperature in the CdSe/CdS dot/rod system is rather complex with multiple processes contributing to a non-radiative recombination[46] which can be favored or hindered by lower temperatures. A difference in PL intensity with temperature between the building blocks of two different CdSe core sizes can also be observed in the individual single component aerogel networks (see Figure S8). While the small core aerogel shows a more or less steady increase of PL intensity at lower temperatures, the large core aerogel shows a slight loss in intensity at moderate temperatures (down to ca. 150 K) to only then increase with decreasing temperature (Figure S8). The interplay of these two behaviors results in the effect observed in the mixed aerogel network of both building blocks. Here, the intensity of the green emission (emanating from the small core part of the network) compared to the red

emission (from the large core part) increases to roughly this temperature of 150 K to then decrease again down to 77 K below which it stays constant and comparable to the ratio of green to red emission observed at room temperature. The PL kinetics likewise are very similar to the measurements of the single component networks described above. A slight decrease in PL lifetime is seen down to ca. 80 K and below that, a drastic increase with a split into two processes can be observed. These measurements taken at the emission maxima of one of the building blocks are very much in line with the measurements of the networks formed solely from the respective building block as displayed in Figure 6D. This is also true for the PL decay behavior of mixed networks assemble from other ratios of SC and LC building blocks, as shown in Figure S9. This again reinforces the point that the emission properties are mostly governed by the CdSe core within these CdSe/CdS dot/rod aerogel networks. The effect of increased PL lifetimes between individual building blocks and assembled networks as reported earlier could likewise be confirmed in this study and may be attributed to the CdS-to-CdS connection within the network enabling further delocalization of the excited electron[8,43] as has

Figure 6. Temperature-dependent optical properties of CdSe/CdS dot/rod NC-based aerogel network consisting of a 1/1 molar ratio small CdSe core (2.0 nm) and large CdSe core (3.9 nm) building blocks. (A) Emission spectra at different temperatures and PL decay measured at the (B) higher energy (small cores, marked blue in panel A) emission peak, corresponding to detection at 525 nm (4 K)-555 nm (295 K), and (C) low energy (large cores, marked red in panel A) emission peak, corresponding to detection at 590 nm (4 K)–615 nm (295 K). (D) PL lifetimes extracted from the decay curves in panel B and C compared to PL lifetimes of aerogels based on one NC building block only.

similarly been demonstrated by increasing the length of the CdS rod-shaped shell.[59] An interaction between building blocks of different core sizes and therefore different band gaps within a mixed network of these two components with regards to emission color or cryogenic PL kinetics could not be observed here.

Conclusions

In summary, CdSe/CdS dot/rod-based aerogel networks were synthesized, and the optical properties of these networks produced starting from two differently sized CdSe cores were investigated. In this context, the known effect of prolonged photoluminescence lifetimes caused by the network formation could be confirmed also for the much smaller CdSe core samples. For the first time the cryogenic PL properties of these networks and their building blocks have been investigated. While the general temperature dependent PL behavior was similar between CdSe QDs, CdSe/CdS dot/rods and CdSe/CdS dot/rod-based aerogel networks, distinct differences from individual NCs to interconnected NC networks could be found. Namely, a remarkably slow dark exciton recombination was observed, which might appear due to the process of aerogel fabrication. The two investigated nanoparticles were subsequently assembled into mixed networks of controlled ratios presenting a convenient approach to color tuning of the macroscopic aerogel networks, as the emission color of the mixed networks can be controlled solely by the mixture of the individual components and no additional interaction between the two differently emitting building blocks during network formation was found. This underlines the governing effect of the CdSe cores on the overall optics of the mixed CdSe/CdS dot/rod aerogel networks.

Experimental Methods

Chemicals

Tri-*n*-octylphosphine oxide (TOPO), Sulfur, 3-mercaptopropionic acid (MPA), potassium hydroxide, methanol, chloroform and hydrogen peroxide (35% aqueous solution) were purchased from Sigma Aldrich. Cadmium oxide and selenium were purchased from Alfa Aesar. Octadecylphosphonic acid and Hexylphosphonic acid were purchased from PCI Synthesis. Tri-*n*-octylphosphine (TOP) was purchased from ABCR. Toluene and acetone were purchased from Merck. All chemicals were used without further purification.

Synthesis of CdSe/CdS Building Blocks

The synthesis of the CdSe cores and the CdSe/CdS dot/rods was performed along with established literature methods.[8,60]

Briefly, 180 mg CdO, 840 mg ODPA and 9 g TOPO were degassed at 150 °C and then heated to 300 °C under nitrogen. 5.4 mL TOP were injected, and the temperature was raised to 350 °C. At this point, a solution of Se in TOP (0.174 g Se in 5.4 mL TOP) was quickly injected, and the reaction mixture was kept at this temperature until the desired size of CdSe NCs was reached (10 s for small cores

ChemPhysChem

Research Article
doi.org/10.1002/cphc.202100755

**Chemistry
Europe**
European Chemical
Societies Publishing

and 4.5 min for large cores respectively). The CdSe NCs were separated and cleaned by repeated precipitation with methanol and dispersion in toluene.

For CdSe/CdS dot/rods 60 mg CdO, 280 mg ODPA, 80 mg HPA and 3 g TOPO were degassed at 150 °C and then heated to 300 °C under nitrogen. 1.8 mL TOP were injected, and the temperature was raised to 350 °C. A solution of S in TOP (0.13 g S in 1.8 mL TOP) containing 80 nmol of CdSe core NCs (as determined by optical spectroscopy)[61] was injected swiftly. The reaction mixture was kept at this temperature for 8 min and then cooled down. The particles were collected and cleaned by repeated precipitation with methanol and dispersion in toluene. Each sample was finally dispersed in 5 mL toluene for storage.

Phase Transfer of CdSe/CdS Building Blocks

The CdSe/CdS dot/rods were phase transferred *via* ligand exchange to MPA.[62,63] 4.5 mL of CdSe/CdS dot/rod solution was added to a phase transfer solution containing 250 μL MPA and 0.2 g KOH in 10 mL MeOH. This mixture was shaken overnight, the NCs were separated by centrifugation and dispersed in 0.1 M KOH. This solution was cleaned of organic contaminants by the addition of 3 mL chloroform and 10 mL acetone. The NCs were again separated by centrifugation and dispersed in 0.01 M KOH. The Cd^{2+} concentration was measured via atom absorption spectroscopy (AAS) and adjusted to 3.6 g/L.

Gelation and Drying of CdSe/CdS Networks

CdSe/CdS dot/rod based networks were produced via oxidative removal of the ligands.[8] Small amounts of hydrogen peroxide (75 μL 0.035 % solution) were added to 800 μL of aqueous CdSe/CdS dot/rod solution. For mixtures of the two CdSe/CdS dot/rods (small core and large core) the respective volumina were calculated using the particle concentration as obtained from the Cd^{2+} concentration and the dot/rod size determined by TEM. These gelation mixtures were heated to 80 °C for 1 min and then kept undisturbed in the dark until a syneresis is visible. The gels are washed by repeated replacement of the supernatant by fresh solvent, first with water and later acetone. After the completed solvent exchange to water-free acetone, the gels can be converted to aerogels by supercritical drying using a critical point dryer (Quorum Technologies E3100). In this, the solvent is first thoroughly exchanged to liquid CO_2 which is afterwards brought to 35 °C at 75 bar (above its critical point). The CO_2 is subsequently released from the dryer to yield NC-based aerogels.

Optical Characterization

Optical spectroscopy was performed using an Edinburgh Instruments FLS 1000. For time-resolved measurements the samples were excited using an Edinburgh Instruments EPL-450 (445.1 nm wavelength, 60 ps pulse width) with a repetition rate of 100 kHz if not stated otherwise, scattered excitation light was filtered out using a colored glass filter. Samples were measured in either 3 mL quartz cuvettes (Hellma Analytics) for solutions or in demountable quartz cuvettes (Hellma Analytics) for solid samples. For temperature-resolved measurements, this spectrometer was coupled with an Oxford Instruments OptistatCF cryostat cooled either by liquid nitrogen or liquid helium with the sample in helium gas. In this case, solid samples were loaded into 1.5 mL quartz cuvettes (Hellma Analytics) and liquids were drop-cast onto quartz glass slides. Time-resolved PL decays were fitted by a monoexponetial decay ($f(x) = A\, e^{-\tau/t} + B$) to extract the PL lifetimes (τ). Quantum yield

and absorption measurements were performed using an Edinburgh Instruments integration sphere using 3 mL quartz cuvettes (Hellma Analytics) or Edinburgh Instruments Teflon solid sample holders with quartz cover slides. Quantum yields were calculated using the integrated area of the scattered excitation peak and the integrated area of the emission peak in the integrating sphere measured with and without the sample. Sample absorption was measured by moving excitation and emission monochromator in synchronous and calculating the difference with and without a sample in the integrating sphere. Absorption measurements of colloidal solutions were performed using an Agilent Cary 5000 spectrometer using 3 mL quartz cuvettes. AAS measurements were performed using a Varion AA140, samples were dissolved in aqua regia prepared from AAS grade acids.

Electron Microscopy

TEM measurements were performed using a FEI Technai G2 F20. Samples were drop-cast onto carbon foil on copper grids (Quantifoil), for aerogel samples small amounts of aerogel were dispersed in acetone by ultrasonication for 5 seconds before drop-casting.

Conflict of Interest

The authors declare no conflict of interest.

[1] T. Gacoin, L. Malier, J. P. Boilot, *Chem. Mater.* **1997**, *9*, 1502.
[2] T. Gacoin, K. Lahlil, P. Larregaray, J. P. Boilot, *J. Phys. Chem. B* **2001**, *105*, 10228.
[3] J. L. Mohanan, I. U. Arachchige, S. L. Brock, *Science* **2005**, *307*, 397.
[4] I. U. Arachchige, J. L. Mohanan, S. L. Brock, *Chem. Mater.* **2005**, *17*, 6644.
[5] C. Ziegler, A. Wolf, W. Liu, A. K. Herrmann, N. Gaponik, A. Eychmüller, *Angew. Chem. Int. Ed.* **2017**, *56*, 13200.
[6] F. Matter, A. L. Luna, M. Niederberger, *Nano Today* **2020**, *30*, 100827.
[7] A. Singh, B. A. Lindquist, G. K. Ong, R. B. Jadrich, A. Singh, H. Ha, C. J. Ellison, T. M. Truskett, D. J. Milliron, *Angew. Chem. Int. Ed.* **2015**, *54*, 14840.
[8] S. Sanchez-Paradinas, D. Dorfs, S. Friebe, A. Freytag, A. Wolf, N. C. Bigall, *Adv. Mater.* **2015**, *27*, 6152.

ChemPhysChem

Research Article
doi.org/10.1002/cphc.202100755

Chemistry Europe
European Chemical
Societies Publishing

[9] A. Freytag, S. Sánchez-Paradinas, S. Naskar, N. Wendt, M. Colombo, G. Pugliese, J. Poppe, C. Demirci, I. Kretschmer, D. W. Bahnemann, P. Behrens, N. C. Bigall, *Angew. Chem. Int. Ed.* **2016**, *55*, 1200.

[10] S. Naskar, A. Freytag, J. Deutsch, N. Wendt, P. Behrens, A. Köckritz, N. C. Bigall, *Chem. Mater.* **2017**, *29*, 9208.

[11] T. Berestok, P. Guardia, M. Ibáñez, M. Meyns, M. Colombo, M. V. Kovalenko, F. Peiró, A. Cabot, *Langmuir* **2018**, *34*, 9167.

[12] D. Zámbó, A. Schlosser, P. Rusch, F. Lübkemann, J. Koch, H. Pfnür, N. C. Bigall, *Small* **2020**, 1906934.

[13] N. C. Bigall, A.-K. Herrmann, M. Vogel, M. Rose, P. Simon, W. Carrillo-Cabrera, D. Dorfs, S. Kaskel, N. Gaponik, A. Eychmüller, *Angew. Chem. Int. Ed.* **2009**, *48*, 9731.

[14] A. Hitihami-Mudiyanselage, K. Senevirathne, S. L. Brock, *ACS Nano* **2013**, *7*, 1163.

[15] K. K. Kalebaila, S. L. Brock, *Z. Anorg. Allg. Chem.* **2012**, *638*, 2598.

[16] A. Hitihami-Mudiyanselage, K. Senevirathne, S. L. Brock, *Chem. Mater.* **2014**, *26*, 6251.

[17] R. Deshmukh, E. Tervoort, J. Käch, F. Rechberger, M. Niederberger, *Dalton Trans.* **2016**, *45*, 11616.

[18] F. J. Heiligtag, N. Kränzlin, M. J. Süess, M. Niederberger, *J. Sol-Gel Sci. Technol.* **2014**, *70*, 300.

[19] Q. Yao, S. L. Brock, *Nanotechnology* **2010**, *21*, DOI 10.1088/0957-4484/21/11/115502.

[20] A. Schlosser, L. C. Meyer, F. Lübkemann, J. F. Miethe, N. C. Bigall, *Phys. Chem. Chem. Phys.* **2019**, *21*, 9002.

[21] W. Liu, A.-K. Herrmann, D. Geiger, L. Borchardt, F. Simon, S. Kaskel, N. Gaponik, A. Eychmüller, *Angew. Chem. Int. Ed.* **2012**, *51*, 5743.

[22] W. Liu, P. Rodriguez, L. Borchardt, A. Foelske, J. Yuan, A.-K. Herrmann, D. Geiger, Z. Zheng, S. Kaskel, N. Gaponik, R. Kötz, T. J. Schmidt, A. Eychmüller, *Angew. Chem. Int. Ed.* **2013**, *52*, 9849.

[23] Z. Fang, Z. Li, G. Yu, *Adv. Mater.* **2020**, DOI 10.1002/adma.202003191.

[24] F. Rechberger, M. Niederberger, *Mater. Horiz.* **2017**, *4*, 1115.

[25] L. Korala, J. R. Germain, E. Chen, I. R. Pala, D. Li, S. L. Brock, *Inorg. Chem. Front.* **2017**, *4*, 1451.

[26] S. Naskar, J. F. Miethe, S. Sánchez-Paradinas, N. Schmidt, K. Kanthasamy, P. Behrens, H. Pfnür, N. C. Bigall, *Chem. Mater.* **2016**, *28*, 2089.

[27] I. U. Arachchige, S. L. Brock, *J. Am. Chem. Soc.* **2007**, *129*, 1840.

[28] F. Lübkemann, J. F. Miethe, F. Steinbach, P. Rusch, A. Schlosser, D. Zámbó, T. Heinemeyer, D. Natke, D. Zok, D. Dorfs, N. C. Bigall, *Small* **2019**, *1902186*, 1902186.

[29] P. Rusch, D. Zámbó, N. C. Bigall, *Acc. Chem. Res.* **2020**, *53*, 2414.

[30] S. Sekiguchi, K. Niikura, N. Iyo, Y. Matsuo, A. Eguchi, T. Nakabayashi, N. Ohta, K. Ijiro, *ACS Appl. Mater. Interfaces* **2011**, *3*, 4169.

[31] F. J. Heiligtag, M. D. Rossell, M. J. Süess, M. Niederberger, *J. Mater. Chem.* **2011**, *21*, 16893.

[32] M. Rosebrock, D. Zámbó, P. Rusch, D. Pluta, F. Steinbach, P. Bessel, A. Schlosser, A. Feldhoff, K. D. J. Hindricks, P. Behrens, D. Dorfs, N. C. Bigall, *Adv. Funct. Mater.* **2021**, 2101628.

[33] R. Wendt, B. Märker, A. Dubavik, A. K. Herrmann, M. Wollgarten, Y. P. Rakovich, A. Eychmüller, K. Rademann, T. Hendel, *J. Mater. Chem. C* **2017**, *5*, 10251.

[34] T. Hendel, V. Lesnyak, L. Kühn, A. K. Herrmann, N. C. Bigall, L. Borchardt, S. Kaskel, N. Gaponik, A. Eychmüller, *Adv. Funct. Mater.* **2013**, *23*, 1903.

[35] T. Mokari, E. Rothenberg, l. Popov, R. Costi, *Science* **2004**, *304*, 1787.

[36] T. Mokari, C. G. Sztrum, A. Salant, E. Rabani, U. Banin, *Nat. Mater.* **2005**, *4*, 855.

[37] J. Schlenkrich, D. Zámbó, A. Schlosser, P. Rusch, N. C. Bigall, *Adv. Opt. Mater.* **2021**, 2101712.

[38] R. Lavieville, Y. Zhang, A. Casu, A. Genovese, L. Manna, E. Di Fabrizio, R. Krahne, *ACS Nano* **2012**, *6*, 2940.

[39] D. Zámbó, A. Schlosser, R. T. Graf, P. Rusch, P. A. Kißling, A. Feldhoff, N. C. Bigall, *Adv. Opt. Mater.* **2021**, DOI 10.1002/adom.202100291.

[40] S. F. Wuister, I. Swart, F. van Driel, S. G. Hickey, C. de Mello Donegá, *Nano Lett.* **2003**, *3*, 503.

[41] F. Di Stasio, J. Q. Grim, V. Lesnyak, P. Rastogi, L. Manna, I. Moreels, R. Krahne, *Small* **2015**, *11*, 1328.

[42] A. Wolf, V. Lesnyak, N. Gaponik, A. Eychmüller, *J. Phys. Chem. Lett.* **2012**, *3*, 2188.

[43] P. Rusch, B. Schremmer, C. Strelow, A. Mews, D. Dorfs, N. C. Bigall, *J. Phys. Chem. Lett.* **2019**, *10*, 7804.

[44] M. G. Lupo, F. Della Sala, L. Carbone, M. Zavelani-Rossi, A. Fiore, L. Lüer, D. Polli, R. Cingolani, L. Manna, G. Lanzani, *Nano Lett.* **2008**, *8*, 4582.

[45] A. Sift, F. Della Sala, G. Menagen, U. Banin, *Nano Lett.* **2009**, *9*, 3470.

[46] X. Wen, A. Sitt, P. Yu, Y. R. Toh, J. Tang, *Phys. Chem. Chem. Phys.* **2012**, *14*, 3505.

[47] M. Grazia Lupo, F. Scotognella, M. Zavelani-Rossi, G. Lanzani, L. Manna, F. Tassone, *Phys. Chem. Chem. Phys.* **2012**, *14*, 7420.

[48] A. S. Blum, M. H. Moore, B. R. Ratna, *Langmuir* **2008**, *24*, 9194.

[49] M. G. Spirin, S. B. Brichkin, V. F. Razumov, *High Energy Chem.* **2015**, *49*, 193.

[50] D. Valerini, A. Cretí, M. Lomascolo, L. Manna, R. Cingolani, M. Anni, *Phys. Rev. B: Condens. Matter Mater. Phys.* **2005**, *71*, 1.

[51] G. Rainò, T. Stöferle, I. Moreels, R. Gomes, J. S. Kamal, Z. Hens, R. F. Mahrt, *ACS Nano* **2011**, *5*, 4031.

[52] A. D. Balan, H. Eshet, J. H. Olshansky, Y. V. Lee, E. Rabani, A. P. Alivisatos, *Nano Lett.* **2017**, *17*, 1629.

[53] Y. P. Varshni, *Physica* **1967**, *34*, 149.

[54] Y. Gao, X. Peng, *J. Am. Chem. Soc.* **2015**, *137*, 4230.

[55] O. Labeau, P. Tamarat, B. Lounis, *Phys. Rev. Lett.* **2003**, *90*, 257404.

[56] L. Biadala, B. Siebers, R. Gomes, Z. Hens, D. R. Yakovlev, M. Bayer, *J. Phys. Chem. C* **2014**, *118*, 22309.

[57] M. G. Lupo, F. Della Sala, L. Carbone, M. Zavelani-Rossi, A. Fiore, L. Lüer, D. Polli, R. Cingolani, L. Manna, G. Lanzani, *Opt. InfoBase Conf. Pap.* **2009**, 1.

[58] B. T. Diroll, C. B. Murray, *ACS Nano* **2014**, *8*, 6466.

[59] A. Hinsch, S. H. Lohmann, C. Strelow, T. Kipp, C. Würth, D. Geißler, A. Kornowski, C. Wolter, H. Weller, U. Resch-Genger, A. Mews, *J. Phys. Chem. C* **2019**, *123*, 24338.

[60] L. Carbone, C. Nobile, M. De Giorgi, F. Della Sala, G. Morello, P. Pompa, M. Hytch, E. Snoeck, A. Fiore, I. R. Franchini, M. Nadasan, A. F. Silvestre, L. Chiodo, S. Kudera, R. Cingolani, R. Krahne, L. Manna, *Nano Lett.* **2007**, *7*, 2942.

[61] W. W. Yu, L. Qu, W. Guo, X. Peng, *Chem. Mater.* **2003**, *15*, 2854.

[62] T. Kodanek, H. M. Banbela, S. Naskar, P. Adel, N. C. Bigall, D. Dorfs, *Nanoscale* **2015**, *7*, 19300.

[63] H. G. Bagaria, E. T. Ada, M. Shamsuzzoha, D. E. Nikles, D. T. Johnson, *Langmuir* **2006**, *22*, 7732.